Journal of Alloys and Compounds 816 (2020) 152672

Contents lists available at ScienceDirect

Journal of Alloys and Compounds

journal homepage: http://www.elsevier.com/locate/jalcom

Optimization of synthesis parameters and pressure effect for layered honeycomb ruthenate $SrRu_2O_6$

Lingling Wang [a], Jianan Chu [a, b, c], Bo Gao [d], Jie Pan [e], Wei Li [f], Teng Wang [a, b, g], Jiaxin Feng [a, b, c], Hui Zhang [a, b], Gang Mu [a, b, *], Fuqiang Huang [b, e], Xiaoming Xie [a, b, c]

[a] State Key Laboratory of Functional Materials for Informatics, Shanghai Institute of Microsystem and Information Technology, Chinese Academy of Sciences, Shanghai, 200050, China
[b] CAS Center for Excellence in Superconducting Electronics (CENSE), Shanghai, 200050, China
[c] University of Chinese Academy of Sciences, Beijing, 100049, China
[d] Center for High Pressure Science and Technology Advanced Research, Beijing, 100094, China
[e] State Key Laboratory of High Performance Ceramics and Superfine Microstructure, Shanghai Institute of Ceramics, Chinese Academy of Sciences, Shanghai, 200050, China
[f] Department of Physics and State Key Laboratory of Surface Physics, Fudan University, Shanghai, 200433, China
[g] School of Physical Science and Technology, ShanghaiTech University, Shanghai, 201210, China

ARTICLE INFO

Article history:
Received 14 August 2019
Received in revised form
9 October 2019
Accepted 13 October 2019
Available online 18 October 2019

Keywords:
A1. $SrRu_2O_6$
A2. pressure effect
B2. synthesis parameters

ABSTRACT

Layered honeycomb compound $SrRu_2O_6$ has drawn great attentions because of the unconventional magnetism with a rather high Ne′el temperature and small ordered moments. Here we report the optimization of synthesis parameters for $SrRu_2O_6$ samples based on the hydrothermal method. The synthesis conditions were tuned carefully in terms of reaction temperature, time of duration, alkalinity and so on. The resultant samples were characterized using the scanning electron microscope, powder x-ray diffractometer, magnetic susceptibility measurements and pressure. We found that $SrRu_2O_6$ can be synthesized at the temperature as low as 140 °C and an appropriate long reaction time can increase the grain size to about 20 μm. The shrinkage of the crystal lattice under high pressure shows an anisotropic behavior. Moreover, the band gap decreases with the increase of the pressure up to 3.0 GPa. Our results here supply an important platform for the further investigations of this system.

1. Introduction

Recently, honeycomb ruthenate $SrRu_2O_6$, which has a quasi-two-dimensional crystal structure with the space group $P\overline{3}1m$, attracted intensive investigations due to its' interesting magnetic properties [1–11]. G-type antiferromagnetic (AF) ordering with a rather high Ne′el temperature $T_N = 565$ K was confirmed by magnetization and neutron powder diffraction measurements [2,3]. Interestingly, this material was found to be a unique system with high Ne′el temperature but small ordered moments because of the coexistence of localized and itinerant electrons [4]. Similar coexistence of large local moments and small ordered magnetic moments was only reported in Fe-based superconductors [12,13]. From the structural point of view, this compound reveals the $PbSb_2O_6$-type structure, which consists of alternating layers of edge-sharing RuO_6 octahedra and interlayed Sr^{2+} ions in a hexagonal unit cell [1] (see Fig. 1a). On the other hand, exploring new classes of superconducting materials with the transition temperature T_c comparable to, or greater than, the cuprate [14,15] and iron-based superconductors [16,17] is one of the major scientific challenges in the field of condensed matter physics and material science. Many efforts from both the experimental and theoretical sides were made to resolve this issue [18–22]. In the unconventional superconducting systems like cuprates and Fe-based superconductors, magnetism and superconductivity were found to be closely related and AF fluctuation was believed to be the glue in the formation of Cooper pairs [7,23]. By combining the behaviors of cuprates and heavy fermion superconductors, a positive correlation between the superconducting transition temperature T_c and the strength of the interaction between the nearest neighbor local moments in their parent AF state was revealed by Pines and it was

---

* Corresponding author. State Key Laboratory of Functional Materials for Informatics, Shanghai Institute of Microsystem and Information Technology, Chinese Academy of Sciences, Shanghai, 200050, China
E-mail address: mugang@mail.sim.ac.cn (G. Mu).

https://doi.org/10.1016/j.jallcom.2019.152672
0925-8388/© 2019 Elsevier B.V. All rights reserved.

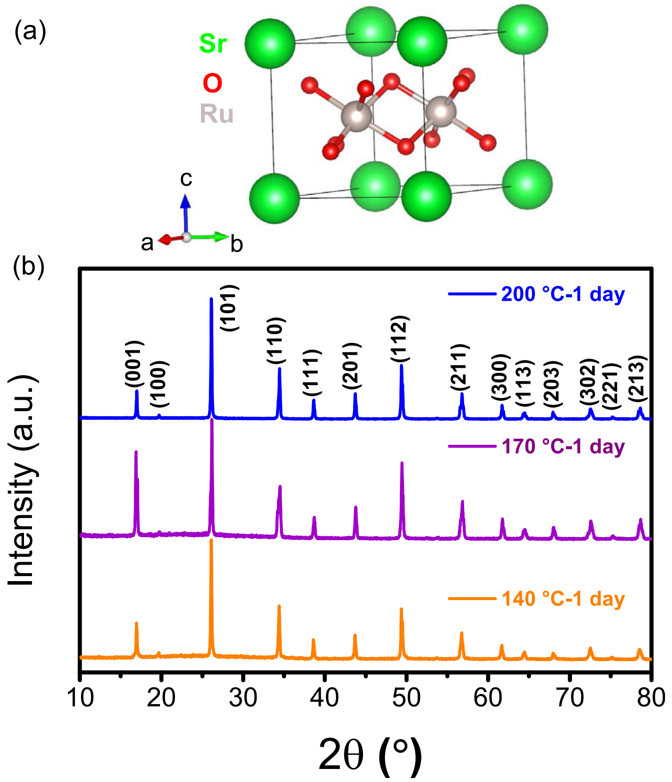

Figure 1. (color online) (a) Structure of $SrRu_2O_6$. (b) Powder X-ray diffraction patterns of $SrRu_2O_6$ synthesized at different temperatures. All the peaks can be indexed to the honeycomb structure of $SrRu_2O_6$. No impurity phase can be detected.

believed that a material with a high Ne′el temperature had the potential to become a high-T_c superconductor when its properties were tuned by doping and/or pressure [24]. From this point of view, the $SrRu_2O_6$ material is also worth the in-depth investigations because of the high value of T_N. Moreover, because of the layered structure, the AF order may be easily destroyed by quantum regulations, which is conducive to the occurrence of superconductivity. Actually, the potential to become the parent of a new superconductor of this compound has been pointed out by the theorists [7]. Currently, this compound can only be prepared by the hydrothermal method. However, a detailed investigation for the optimization of synthesis parameters and quantum regulations on this system is still lacking.

In this paper, we report the optimization of the hydrothermal synthesis conditions and the structure characterizations of the honeycomb ruthenate $SrRu_2O_6$. It is found that the reaction temperature, time of duration and alkalinity of the solution can affect the purity and crystal size of the products. Moreover, the mechanical pressure shows an anisotropic effect on the crystal structure. The electronic structure can be influenced and the band gap is found to be suppressed by the pressure.

2. Materials and methods

2.1. Synthesis of $SrRu_2O_6$

$SrRu_2O_6$ samples was synthesized by hydrothermal method [1]. We have tuned the reaction conditions including heating temperature, time of duration, alkalinity and so on. In a typical synthesis, 1 mmol SrO and 1 mmol $KRuO_4$ were successively added into the 10 mL deionized water by stirring for 30 min, and then the solution was poured into 25 mL Teflon-lined autoclave and heated up to 200 °C for 1 day. The reacted precipitate was cleaned with deionized water and 15 mL dilute HCl aqueous solution to remove $SrCO_3$ (a by-product of excess SrO). Finally, dried black powders of $SrRu_2O_6$ polycrystalline samples were obtained. We have also tried lowering the reaction temperature to 140 °C, 170 °C for 1 day to optimize hydrothermal synthesis conditions. In addition, we found that the product was influenced by the alkalinity of hydrothermal reaction solution with adding 30, 60, and 120 mmol NaOH. In order to obtain large sized $SrRu_2O_6$ crystals, increasing the hydrothermal reaction time (5, 8, 18 days at 200 °C) was also adopted. The detailed information about the agent amounts and reaction conditions in our experiments are summarized in Table 1 and Table 3.

2.2. Characterization and property measurements

The crystal structure was checked by powder x-ray diffraction (PXRD) measurements at room temperature using a DX-2700 diffractometer with Cu K_α radiation. High pressure x-ray diffraction experiments with a wavelength of 0.4337 Å were performed in a symmetrical diamond anvil cell (DAC) at 13-BMC of the Advanced Phonon Source (APS), Argonne National Laboratory (ANL). Neon was used as the pressure transmitting medium. Pressure was determined by using the ruby fluorescence method. The morphology of the samples was characterized by JSM-6510 scanning electron microscope (SEM). The dc magnetization measurements were done with a magnetic property measurement system (Quantum Design, MPMS 3).

2.3. First-principle calculations

The first-principles calculations presented in this work were

Table 1
Raw materials, the reaction conditions (including temperature and time), and the yield for the material synthesis.

SrO (mmol)	$KRuO_4$ (mmol)	H_2O (mL)	Temperature (°C)	Time (day)	Yield (%)
1.0	1.0	10	140	1	16.5
1.0	1.0	10	170	1	26.1
1.0	1.0	10	200	1	71.1
1.0	1.0	10	200	5	76.2
1.0	1.0	10	200	8	75.3
1.0	1.0	10	200	18	73.2

Table 2
Lattice parameters for $SrRu_2O_6$ obtained under different synthesis conditions.

Temperature (oC)	Time (day)	a (Å)	c (Å)
140	1	5.2053	5.2209
200	1	5.2069	5.2299
200	8	5.2076	5.2278

Table 3
Raw material, PH values and the corresponding products for the material synthesis. The reaction condition is fixed to 200 °C and 1 day.

NaOH (mmol)	SrO (mmol)	$KRuO_4$ (mmol)	H_2O (mL)	pH value	Products
0	1.0	1.0	10	13.3	$SrRu_2O_6$
30	1.0	1.0	10	14.5	$Sr_2Ru_3O_{10}$
60	1.0	1.0	10	14.8	$Sr_2Ru_3O_{10}$+$SrRuO_3$
120	1.0	1.0	10	15.1	$SrRuO_3$

Table 4
Lattice parameters for $SrRu_2O_6$ under different pressures.

Pressure (GPa)	a (Å)	c (Å)
0	5.2044	5.2163
0.7	5.2010	5.1872
3.0	5.1875	5.0961

performed using the all-electron full potential linear augmented plane wave plus local orbitals method [25] as implemented in the WIEN2K code [26]. The exchange-correlation potential was calculated using the generalized gradient approximation as proposed by Pedrew, Burke, and Ernzerhof [27]. The atomic internal coordinates were optimized with fixed the lattice constants based on the experimental parameters (see Table 4 in the main text).

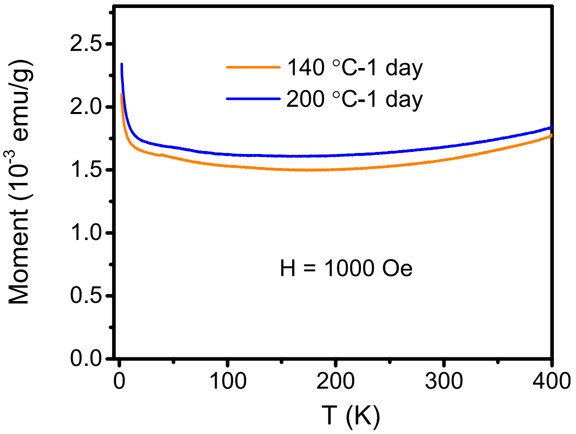

Fig. 2. Magnetic susceptibility as a function of temperature for two samples synthesized under different conditions.

3. Results and discussion

3.1. Effect of reaction temperature

The hydrothermal reactions were carried out at three different temperatures for a fixed duration time, 1 day. The detailed information was summarized in Table 1 (see the first three rows). The crystal structure and phase purity of the products were checked using the PXRD measurements at room temperature. The resultant diffraction patterns can be seen in Fig. 1b. The products are rather pure and all the diffraction peaks can be indexed to the honeycomb $PbSb_2O_6$-type structure with the space group $P\overline{3}1m$ as shown in Fig. 1a.

It is notable that even at the temperature as low as 140 °C, the pure-phase $SrRu_2O_6$ can be synthesized. However, the yield of the product is found to be lower when the reaction temperature is lower, as shown in the last column of Table 1. The yield of the product is about 75% at 200 °C. The loss of the product mainly comes from the cleaning and collecting process of the precipitated product. Thus the reaction temperature 200 °C is sufficient and will be adopted in the following investigations on the effects of reaction time and the solution alkalinity.

We studied the magnetic property of samples synthesized at different temperature. In Fig. 2, we show the magnetic susceptibility data of two samples obtained at 140^{o}C and 200 °C. The two sets of data reveal the similar behavior and values in the whole temperature region we measured, which indicates that the reaction temperature has a small influence on the magnetic property of the material. The evolution tendency as a function of temperature is consistent with the previous report and the small upturn in the low temperature has been attributed to uncompensated spins or tiny impurities [1].

3.2. Effect of reaction time

In order to improve the phase formation and crystal size, we tried the scenario with a much longer reaction time. The sample

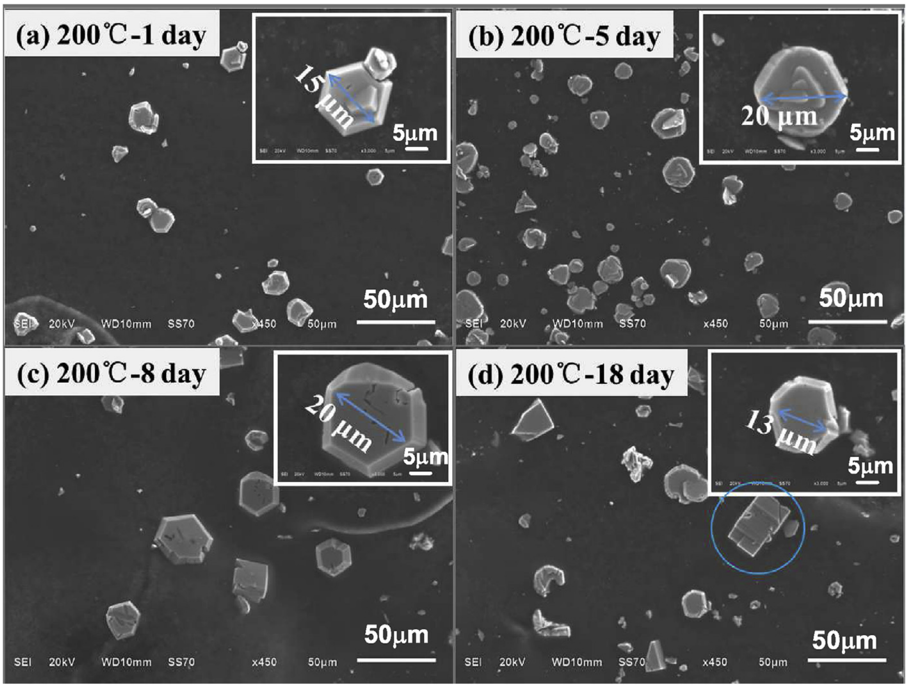

Fig. 3. The surface pictures of the samples taken with the SEM with different reaction time. (a) For 1 day. (b) For 5 days. (c) For 8 days. (d) For 18 days.

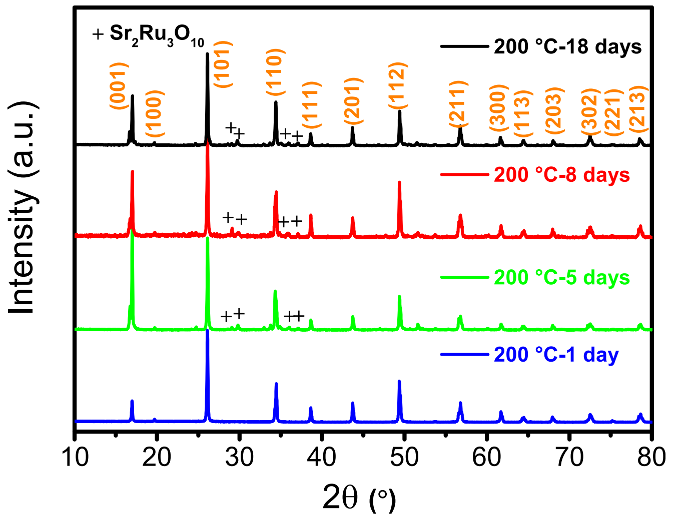

Fig. 4. Powder X-ray diffraction patterns of $SrRu_2O_6$ synthesized with different reaction time. Mains peaks can be indexed to the honeycomb structure of $SrRu_2O_6$. Small amounts of impurity phase from $Sr_2Ru_3O_{10}$ are marked by the plus signs (+).

morphology was characterized using the scanning electron microscope. As can be seen in Fig. 3, typically the small crystals show the hexagonal shape, which is consistent with the space group of $SrRu_2O_6$. The maximum crystal size for the sample with the reaction time of 1 day is about 15 μm (see Fig. 3a). As the reaction time was raised to 5 days, the crystals can grow to a larger size, with the maximum value 20 μm (see Fig. 3b). For the case of 8 days, it was much easier to find a large grain of about 20 μm in a collection of powder samples (see Fig. 3c), indicating a gradual increase for the distribution of large crystals. With the reaction time further increased, for example 18 days, the grain size became smaller (see Fig. 3d). We note here that the maximum grain size around 20 μm in the present work is several times larger than that reported by other groups. In the work of Hiley et al. [1,2], the size of crystal grains is smaller than 10 μm.

Moreover, some grains with a rectangle shape, instead of the hexagonal one, emerges when the reaction time is increased (see the one denoted by the blue circled in Fig. 3d). The emergence of a small amount of second phase was further confirmed by the PXRD measurements. As shown in Fig. 4, besides $SrRu_2O_6$ as the main phase, small diffraction peaks from the impure phase were also detected (see the plus signs). A careful analysis showed that the positions of the diffraction peaks for the impure phase was rather consistent with the $Sr_2Ru_3O_{10}$ compound, which shows a monoclinic symmetry [28,29]. The fact that the grain shape in the blue circle in Fig. 3d is also very similar to the SEM picture of the $Sr_2Ru_3O_{10}$ (see Fig. 5b) enhances the reliability of our judgment.

We also checked the possible influences of the synthesis temperature and time on the detailed structure parameters. The lattice parameters are obtained by fitting the PXRD data. In Table 2, we present the results of the samples synthesized with three different conditions: 140 °C-1 day, 200 °C-1 day and 200 °C-8 day. From the data we can see that these synthesis conditions have little effect on the crystal structure of materials: the *a*- and *c*-axis parameters change by only 0.04% and 0.2% respectively. The reaction temperature shows a relatively larger influence than the duration time.

3.3. Effect of solution alkalinity

By adding an additional amount of NaOH, we adjusted the alkalinity of the reaction solution. As summarized in Table 3, 30 mmol, 60 mmol, and 120 mmol NaOH were added to the solution and the pH value can be tuned from 13.3 to 15.1. The reaction temperature and time were fixed to 200 °C and 1 day respectively. From the PXRD patterns shown in Fig. 5a, we can see that with 30 mmol NaOH added the products transformed to the monoclinic $Sr_2Ru_3O_{10}$ (2-3-10) compound [28,29]. As the amount of NaOH was increased to 60 mmol, the cubic $SrRuO_3$ (1-1-3) phase [30] began to emerge and we obtained a mixture of the 2-3-10 and 1-1-3 phases. Only the 1-1-3 phase can be seen when the amount of NaOH was further increased to 120 mmol. Fig. 5b and c displays the SEM pictures for the obtained samples with the NaOH amounts of 30 mmol and 120 mmol respectively. The shape of the grain shown in Fig. 5b is very similar to that observed in the 18 days condition (see the circled grain in Fig. 3d), which can be attributed to the $Sr_2Ru_3O_{10}$ compound in combination with the PXRD results. As for the products in Fig. 5c, it is a collection of cubic grains being consistent with the $SrRuO_3$ phase.

3.4. Effect of mechanical pressure

In order to regulate its electronic state, we carried out various

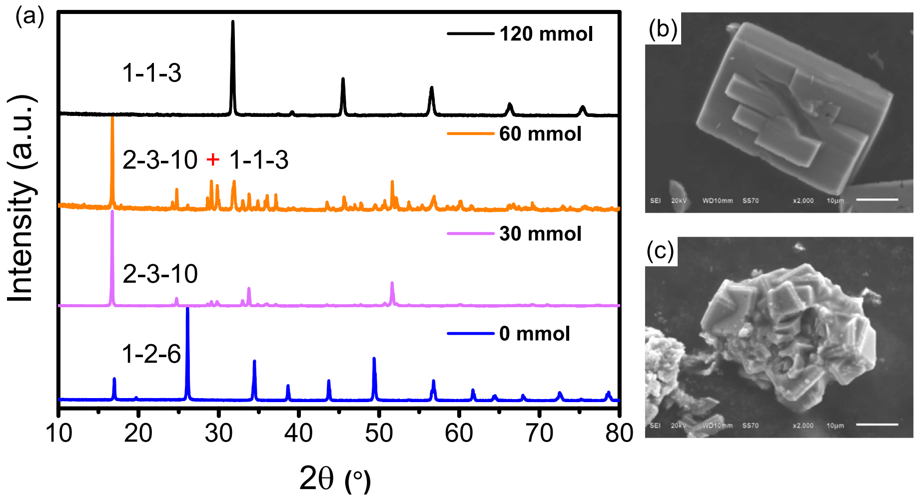

Fig. 5. (a) Powder X-ray diffraction patterns of the resultant products synthesized with different solution alkalinity. Three phases, $SrRu_2O_6$ (1-2-6), $Sr_2Ru_3O_{10}$ (2-3-10), $SrRuO_3$ (1-1-3), can be formed under different conditions. (b)–(c) The SEM pictures for the products obtained with 30 mmol and 120 mmol NaOH respectively.

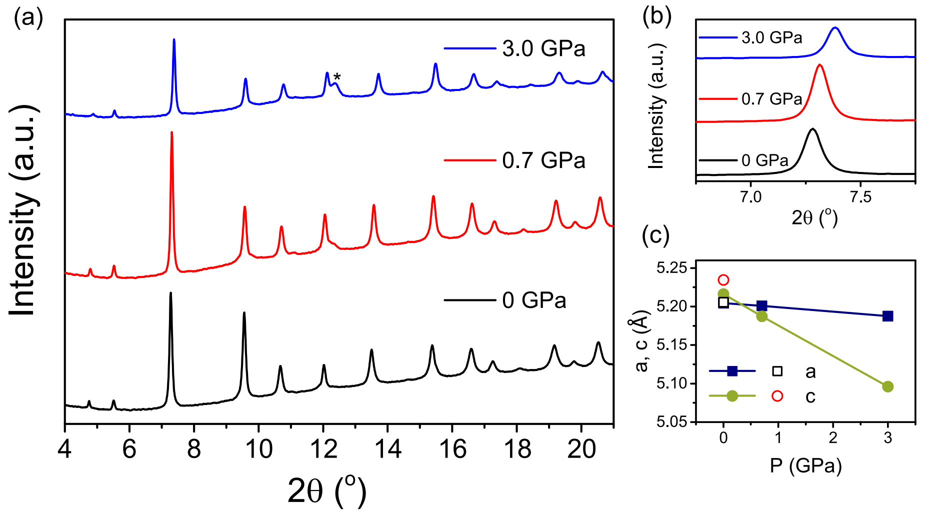

Fig. 6. (a) Powder X-ray diffraction patterns of the $SrRu_2O_6$ compound under different mechanical pressures. The small peak indexed by the asterisk comes from the gasket in the high-pressure cell. (b) An enlarged view for the PXRD pattern near the main peak. The peak moves to right with the increase of pressure. (c) Pressure dependence of the lattice parameters. The solid symbols are from this work and the open ones are cited from reference [1].

doping experiments on this material, including doping Ca and Ba on the site of Sr, doping Co, Ni, Mn, V on the site of Ru, and so on. Unfortunately, it seems that this material is very stable and none of these dopants can be substituted to the lattice successfully. Alternatively, we tuned the crystal and electronic structure of $SrRu_2O_6$ by applying the mechanical pressure. The PXRD was measured using the synchrotron radiation X-ray with the wavelength of 0.4337 Å. As shown in Fig. 6a, the distribution of the diffraction peaks remained unchanged with the pressure up to 3.0 GPa, and all the peaks can be indexed to the structure of $SrRu_2O_6$. Meanwhile, the positions of the peaks shifted slightly to the right direction, indicating a shrinkage of the unit cell induced by the pressure. This tendency can be observed more clearly in the enlarged view of the PXRD data, which is shown in Fig. 6b. As the pressure was further increased to about 6 GPa, additional diffraction peaks began to appear (data not shown here) indicating a reduction of the lattice symmetry. Due to the limited number and intensity of the peaks, currently it is difficult to index them.

By using the software FullProf, we analyzed the PXRD data and obtained the lattice parameters. The results were represented in Fig. 6c and Table 4. The lattice parameters under ambient pressure are roughly consistent with the previous report [1] and the result

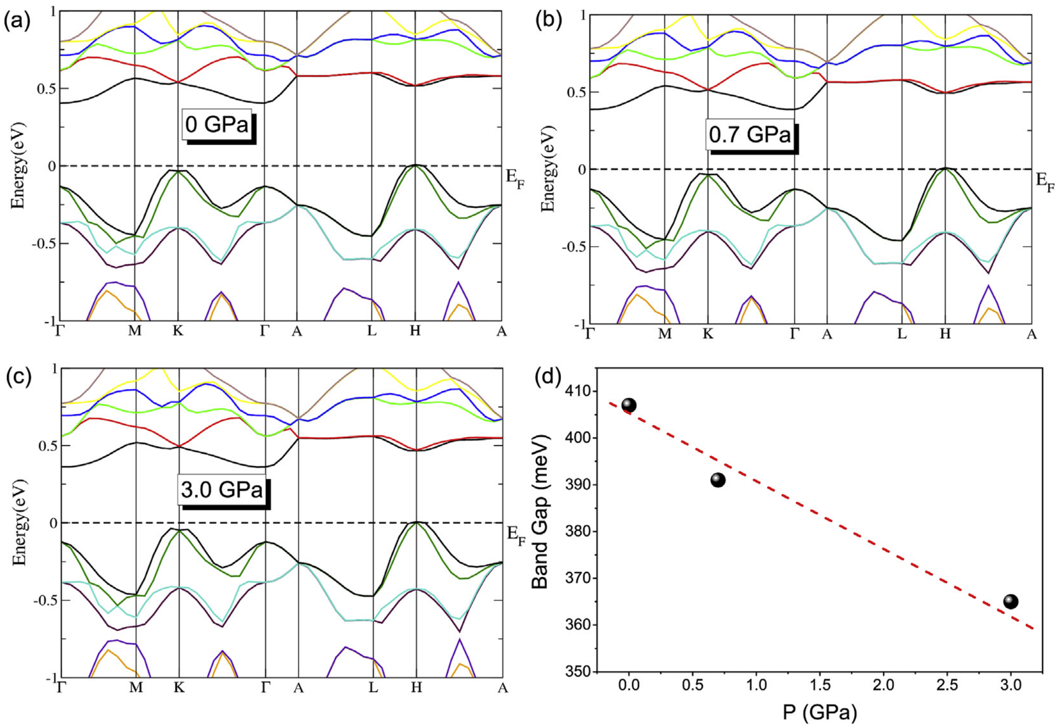

Fig. 7. The electronic band structure of G-type AF state for $SrRu_2O_6$ under the pressures of (a) P = 0 Gpa, (b) P = 0.7 GPa, and (c) x = 3.0 GPa. (d) The pressure dependence of the energy band gap. The dashed straight line is a guide for eyes.

in Table 2. With the increase of pressure, both the *a*- and *c*-axis lattice parameters displayed a roughly linear decrease. Quantitatively, the *a*-axis lattice parameter decreased slightly with the pressure, accounting for a shrinkage of about 0.3% under 3.0 GPa. In contrast, the *c*-axis lattice parameter was suppressed more obviously, by 2.3% under the same pressure. Such an anisotropic behavior for the lattice shrinkage under pressure has been observed in other layered materials [31–33], which reflects the anisotropy of the chemical bond strength in these compounds. Typically, the chemical bond within one layer is rather strong, while that between neighboring layers is weak. This anisotropic response of the crystal structure on the pressure is expected to affect the electronic structure of this material.

In Fig. 7a–c, we show the energy band structures in the G-type AF state [2,3] under various pressures. The low energy features of electronic band structure remain almost unchanged with the applied pressure. As shown in Fig. 7d, the main effect of the pressure is to suppress the energy band gap. The magnitude of the energy band gap decreases almost linearly as increasing the pressure from 0 GPa (407 meV) to 3.0 GPa (365 meV). Following this tendency, the band gap should be closed at around 29 GPa without the occurrence of the structural phase transition. However, we have observed the reduction of the lattice symmetry under the pressure of about 6 GPa (data not shown here), suggesting that the structural phase transition has taken place at a higher pressure.

4. Conclusions

In this work, layered honeycomb compound $SrRu_2O_6$ was synthesized by the hydrothermal method. Reaction temperature, reaction time, and solution alkalinity were tuned to explore the optimum phase forming condition of this compound. It is found that this compound can be synthesized at the temperature as low as 140 °C and an appropriate long reaction time can increase the grain size. Further increasing the reaction time and the addition of alkalinity will lead to the formation of other Ru-related compounds like $Sr_2Ru_3O_{10}$ or $SrRuO_3$. Moreover, the application of mechanical pressure can suppress the size of the *c*-axis lattice parameter more severely than the *a*-axis one. The band gap was found to be suppressed by the pressure.

Declaration of competing interest

The authors declare that they have no known competing financial interests or personal relationships that could have appeared to influence the work reported in this paper.

Acknowledgments

This work is supported by the Youth Innovation Promotion Association of the Chinese Academy of Sciences (No. 2015187), the National Natural Science Foundation of China (No. 11204338), and the “Strategic Priority Research Program (B)” of the Chinese Academy of Sciences (No. XDB04040300). Portions of this work were performed at GeoSoilEnviroCARS (The University of Chicago, Sector 13), Advanced Photon Source (APS), Argonne National Laboratory. GeoSoilEnviroCARS is supported by the National Science Foundation - Earth Science (No. EAR - 1634415) and Department of Energy-GeoSciences (No. DE-FG02-94ER14466). This research used resources of the Advanced Photon Source, a U.S. Department of Energy (DOE) Office of Science User Facility operated for the DOE Office of Science by Argonne National Laboratory (No. DE-AC02-06CH11357).

Appendix A. Supplementary data

Supplementary data to this article can be found online at https://doi.org/10.1016/j.jallcom.2019.152672.

References

[1] C.I. Hiley, M.R. Lees, J.M. Fisher, D. Thompsett, S. Agrestini, R.I. Smith, R.I. Walton, Angew. Chem. Int. Ed. 53 (17) (2014) 4423–4427.

[2] C.I. Hiley, D.O. Scanlon, A.A. Sokol, S.M. Woodley, A.M. Ganose, S. Sangiao, J.M. De Teresa, P. Manuel, D.D. Khalyavin, M. Walker, M.R. Lees, R.I. Walton, Phys. Rev. B 92 (2015) 104413.

[3] W. Tian, C. Svoboda, M. Ochi, M. Matsuda, H.B. Cao, J.-G. Cheng, B.C. Sales, D.G. Mandrus, R. Arita, N. Trivedi, J.-Q. Yan, Phys. Rev. B 92 (2015) 100404 (R).

[4] S. Okamoto, M. Ochi, R. Arita, J. Yan, N. Trivedi, Sci. Rep. 7 (2017) 11742.

[5] M. Ochi, R. Arita, N. Trivedi, S. Okamoto, Phys. Rev. B 93 (2016) 195149.

[6] D.J. Singh, Phys. Rev. B 91 (2015) 214420.

[7] D. Wang, W.-S. Wang, Q.-H. Wang, Phys. Rev. B 92 (2015) 075112.

[8] S. Streltsov, I.I. Mazin, K. Foyevtsova, Phys. Rev. B 92 (2015) 134408.

[9] A. Hariki, A. Hausoel, G. Sangiovanni, J. Kuneš, Phys. Rev. B 96 (2017) 155135.

[10] Y.S. Ponosov, E.V. Komleva, D.A. Zamyatin, R.I. Walton, S.V. Streltsov, Phys. Rev. B 99 (2019) 085103.

[11] H. Suzuki, H. Gretarsson, H. Ishikawa, K. Ueda, Z. Yang, H. Liu, H. Kim, D. Kukusta, A. Yaresko, M. Minola, J.A. Sears, S. Francoual, H.C. Wille, J. Nuss, H. Takaki, B.J. Kim, G. Khaliullin, H. Yavas, B. Keimer, Nat. Mater. 18 (2019) 563–567.

[12] P. Hansmann, R. Arita, A. Toschi, S. Sakai, G. Sangiovanni, K. Held, Phys. Rev. Lett. 104 (2010) 197002.

[13] M. Liu, L.W. Harriger, H. Luo, M. Wang, R.A. Ewings, T. Guidi, H. Park, K. Haule, G. Kotliar, S.M. Hayden, P. Dai, Nat. Phys. 8 (2012) 376–381.

[14] J.G. Bednorz, K.A. Müller, Z. Phys. B 64 (2) (1986) 189–193.

[15] H. Maeda, Y. Tanaka, M. Fukutomi, T. Asano, Jpn. J. Appl. Phys. 27 (1988) L209–L210.

[16] Y. Kamihara, T. Watanabe, M. Hirano, H. Hosono, J. Am. Chem. Soc. 130 (2008) 3296–3297.

[17] Z.-A. Ren, W. Lu, J. Yang, W. Yi, X.-L. Shen, Z.-C. Li, G.-C. Che, X.-L. Dong, L.-L. Sun, F. Zhou, Z.-X. Zhao, Chin. Phys. Lett. 25 (6) (2008) 2215.

[18] J. Hu, C. Le, X. Wu, Phys. Rev. X 5 (2015) 041012.

[19] L. Wang, X. Ma, Q.-K. Xue, Supercond. Sci. Technol. 29 (12) (2016) 123001.

[20] A.P. Drozdov, M.I. Eremets, I.A. Troyan, V. Ksenofontov, S.I. Shylin, Nature 525 (2015) 73–76.

[21] M. Somayazulu, M. Ahart, A.K. Mishra, Z.M. Geballe, M. Baldini, Y. Meng, V.V. Struzhkin, R.J. Hemley, Phys. Rev. Lett. 122 (2019) 027001.

[22] A.P. Drozdov, P.P. Kong, V.S. Minkov, S.P. Besedin, M.A. Kuzovnikov, S. Mozaffari, L. Balicas, F. Balakirev, D. Graf, V.B. Prakapenka, E. Greenberg, D.A. Knyazev, M. Tkacz, M.I. Eremets, Nature 569 (2019) 528–531.

[23] D.J. Scalapino, Rev. Mod. Phys. 84 (2012) 1383–1417.

[24] D. Pines, J. Phys. Chem. B 117 (42) (2013) 13145–13153.

[25] D.J. Singh, L. Nordstrom, In: Planewaves, Pseudopotentials, and the LAPW Method, Springer-Verlag, Berlin, 2006.

[26] P. Blaha, K. Schwarz, G. Madsen, D. Kvasnicka, J. Luitz, In: an Augmented PlaneWave + Local Orbitals Program for Calculating Crystal Properties, Technical Univievsity Wien, Austria, 2001.

[27] J.P. Perdew, K. Burke, M. Ernzerhof, Phys. Rev. Lett. 77 (1996) 3865.

[28] C. Renard, S. Daviero-Minaud, F. Abraham, J. Solid State Chem. 143 (2) (1999) 266–272.

[29] T. Marchandier, Q. Jacquet, G. Rousse, B. Baptiste, A.M. Abakumov, J.-M. Tarascon, Chem. Mater. 31 (16) (2019) 6295–6305.

[30] H. Samata, Y. Saeki, S. Mizusaki, Y. Nagata, T. Ozawa, A. Sato, J. Cryst. Growth 311 (3) (2009) 623–626.

[31] S. Margadonna, Y. Takabayashi, Y. Ohishi, Y. Mizuguchi, Y. Takano, T. Kagayama, T. Nakagawa, M. Takata, K. Prassides, Phys. Rev. B 80 (2009) 064506.

[32] J. Zhang, F.L. Liu, T.P. Ying, N. Li, Y. Xu, L.P. He, Y.J. Hong, X.C. Yu, M.X. Wang, J. Shen, W.G. Yang, S.Y. Li, npj Quantum Mater. 2 (2017) 49.

[33] B. Wang, Z.-C. Wang, K. Ishigaki, K. Matsubayashi, T. Eto, J. Sun, J.-G. Cheng, G.-H. Cao, Y. Uwatoko, Phys. Rev. B 99 (2019) 014501.